Available online at www.sciencedirect.com
ScienceDirect
Ceramics International 38 (2012) 517–526
CERAMICS INTERNATIONAL
www.elsevier.com/locate/ceramint

Cleaner production of porcelain tile powders. Granule and green compact characterization

Z. Shu [a,b,*], J. Garcia-Ten [b], E. Monfort [b], J.L. Amoros [b], J. Zhou [c], Y.X. Wang [a]

[a] MOE Key Laboratory of Biogeology and Environmental Geology and School of Environmental Studies, China University of Geosciences, 430074 Wuhan, PR China
[b] Instituto de Tecnología Cerámica, Asociación de Investigación de las Industrias Cerámicas, Universitat Jaume I, 12006 Castellon, Spain
[c] MOE Key Engineering Research Center of Nano-Geomaterials and Faculty of Material Science and Chemical Engineering, China University of Geosciences, 430074 Wuhan, PR China

Received 9 July 2011; accepted 16 July 2011
Available online 26th July 2011

Abstract

A new ceramic powder preparation process, the droplet–powder granulation process (DPGP), was recently proposed in pursuit of energy/water conservation and environment protection for sustainable development of the ceramic industry.

This study characterizes the DPGP granules and resulting pressed green compacts and compares them with those obtained using traditional spray-drying (hereafter SD) and granulation (hereafter G) processes. Powder and granule properties (granule size distribution, flowability, microstructure, yield pressure, etc.), powder pressing behaviour, and green compact properties (microstructure, bending strength, etc.) were determined. The properties of the DPGP powder and the resulting compacts displayed an intermediate performance between those of the powders and compacts obtained by the SD and G processes, demonstrating the feasibility of the DPGP process in the pre-firing stage of porcelain tile manufacture. The study also shows that, in addition to the key spray-mixing step, the subsequent rolling treatment also plays a major role in DPGP granule formation.

Keywords: B. Microstructure-prefiring; B. Porosity; D. Porcelain; Apparent yield pressure; Tiles

1. Introduction

Ceramic powder preparation is a critical process stage in the manufacture of ceramic materials formed by pressing. Ceramic powder properties such as particle, granule, and pore size distribution, as well as flowability and deformability, significantly affect the powder pressing behaviour, not only in die filling but also in compaction during pressing, and can lead to different microstructures and mechanical characteristics in the pressed compacts, which affect subsequent processing [1–4].

Different preparation processes generally produce ceramic powders with different properties. Currently, in the ceramic tile industry, ceramic powders for porcelain tiles are mainly produced by spray drying, after which the compacts are formed by pressing [5]. The technical command of raw material wet milling and the excellent performance of spray-dried powders have led to wide-scale industrial application of the spray-drying process in the last 40 years. However, the high energy and water consumption involved in spray drying, in addition to pollution emissions, remain major issues, especially in developed areas such as European countries [6–8]. Another ceramic powder preparation approach is granulation of dry-milled raw materials, though this has not yet been used in the manufacture of porcelain tiles, where very low porosity in the final product is required.

A new ceramic powder preparation process, the droplet–powder granulation process (hereafter DPGP), has recently been proposed for cleaner ceramic tile manufacture [9]. In the new proposed process, the raw materials are wet milled to slurry, just as in the wet milling step in the spray-drying process. About two-thirds of the slurry is filter pressed, dried, and milled into fine dry powder. The other one-third of the slurry and the as-obtained fine dry powder are sprayed into a tower, where the

* Corresponding author at: MOE Key Laboratory of Biogeology and Environmental Geology and School of Environmental Studies, China University of Geosciences, 430074 Wuhan, PR China.
E-mail addresses: zhushu426@gmail.com, zhushu426@163.com (Z. Shu).

0272-8842/$36.00
doi:10.1016/j.ceramint.2011.07.037

sprayed slurry droplets adsorb the dispersed dry powder to form granules that are then collected, rolled, and dried to form suitable press powder. The new process constitutes an alternative ceramic powder preparation process and, in comparison with spray drying (hereafter SD), as reported in a previous study [9], can significantly reduce emissions of particulate matter into the air (98%), save energy (24%), and reduce water consumption (69%). In the spray-drying process, water is removed by heat treatment in a single step, entailing significant pollution unless high-efficiency corrective measures are applied [6]. In contrast, in the DPGP process, water is removed in three steps: by filter pressing the slurry (removing about 40% of all water, without dust emissions, and recycling the filtered water), drying the filter-pressed cake and, finally, drying the granules, thus providing significant pollution abatement despite involving more process steps.

This study analyses the droplet–powder granulation process (DPGP) and characterizes the properties of the DPGP ceramic powder and resulting green compacts. Ceramic powders were also prepared by SD, the traditional wet route, and by granulation (hereafter G), the traditional dry route. The three types of powder were prepared from the same starting porcelain tile composition. The SD and G powders and the resulting green compacts were characterized and compared with those obtained by the DPGP process.

2. Experimental

2.1. Raw materials

A porcelain tile composition was used, consisting of 35 wt% ball clay (UA-50, VESKO, United Mineral Group), 55 wt% sodium feldspar (ESF501-CG, ESAN ECZACIBASI Group), and 10 wt% quartz (AFS-100, Imerys Group). Fine ground sodium feldspar (0.82 wt% residue on a 63 μm sieve) and quartz (9.80 wt% residue on a 63 μm sieve) were used. Table 1 shows the chemical and mineralogical analysis of the raw materials and the porcelain tile composition used.

Table 1
Chemical and mineralogical analysis of the raw materials and porcelain tile composition used.

	Raw material (wt%)			Porcelain tile composition (wt%)
	Ball clay	Sodium feldspar	Quartz	
Chemical analysis				
SiO_2	64.30	69.50	91.00	69.83
Al_2O_3	23.50	18.00	5.00	18.63
Fe_2O_3	0.96	0.14	0.12	0.43
TiO_2	1.35	0.28	0.08	0.63
CaO	0.20	0.50	0.10	0.36
MgO	0.50	0.20	0.01	0.29
Na_2O	0.50	10.00	0.10	5.69
K_2O	2.10	0.80	2.50	1.43
LOI	6.31	0.50	1.06	2.59
Others	0.28	0.08	0.03	0.15
Total	100.00	100.00	100.00	100.00
Mineralogical analysis				
Illite	24	0	15	10
Kaolinite	38	2	6	15
Quartz	37	10	79	26
Albite	0	87	0	48
Others	1	1	0	1
Total	100	100	100	100

2.2. Ceramic powder preparation processes

Ceramic powders were prepared using three processes: spray drying (SD), droplet–powder granulation (DPGP), and granulation (G). The processes, schematically illustrated in Fig. 1, are briefly described below.

SD: Ball clay was dried and slightly ground by hammer milling. Batch-weighed raw materials were wet mixed in water with 0.2 wt% deflocculant (sodium metasilicate ($Na_2SiO_3{\cdot}5H_2O$) and sodium tripolyphosphate ($Na_5P_3O_{10}$) in a 3:1 ratio by weight), on a solid basis, to prepare slurry with 68 wt% solids content and viscosity of 0.65 Pa s (Gallenkamp viscometer). The slurry was spray dried in a pilot spray dryer to obtain SD ceramic powder with a moisture content of 0.055 kg water/kg dry solid.

DPGP: The same slurry as that of the SD process was used. About 2/3 of the slurry was filter pressed into wet cake; 0.75 wt% flocculant (pure acetic acid), on a solid basis, was used in filter pressing to improve filtering efficiency. The filter-pressed cake was dried and then ground to fine dry powder in a hammer mill with a 200 μm sieve. The remaining one-third of the slurry and as-obtained dry powder were sprayed into a tower as a mixed flow (Fig. 2) of slurry droplets (bottom) and dispersed dry powder (top). In the tower, the

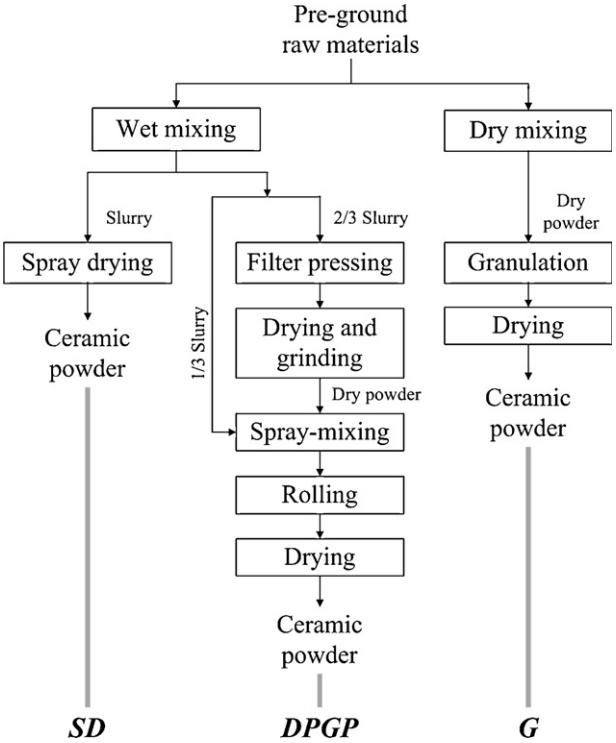

Fig. 1. Flowcharts of the three preparation processes: SD, DPGP, and G.

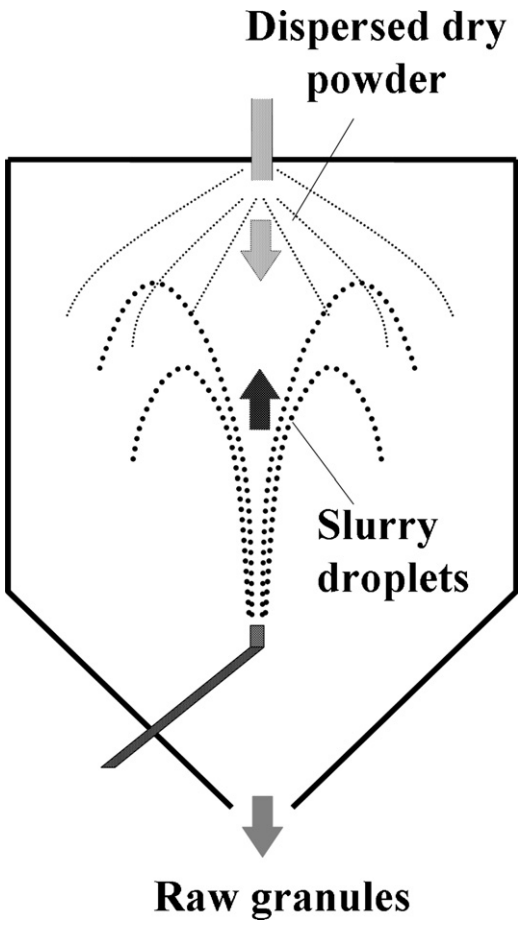

Fig. 2. Granulation principle in DPGP spray-mixing.

slurry droplets continually adsorbed the dispersed dry powder, forming the raw granules, which exited the tower with a moisture content of 0.165 kg water/kg dry solid. The raw granules were then subjected to rolling treatment in a laboratory planet mill (without grinding media) for 30 s, which caused the raw granules to run along the chamber wall, yielding the rolled granules. These were then dried to obtain DPGP ceramic powder with a moisture content of 0.055 kg water/kg dry solid.

G: Ball clay was dried and fine ground by pendulum milling, simulating industrial practice. Batch-weighed raw materials were homogenized and granulated in an intensive mixer (Eirich RO2) to a moisture content of 0.140 kg water/kg dry solid. The resulting granules were then dried to obtain G ceramic powder with a moisture content of 0.055 kg water/kg dry solid.

Ceramic powder was also prepared by the G process, without granulation, as a blank reference.

All the ceramic powders were sieved to remove agglomerates larger than 1000 μm and stored for 24 h to homogenize their moisture content. The particle size distributions (PSDs) of the three powders (Fig. 3) were determined by laser diffraction, using water as dispersing medium. The three powder PSDs may be considered equivalent for the purpose of this study.

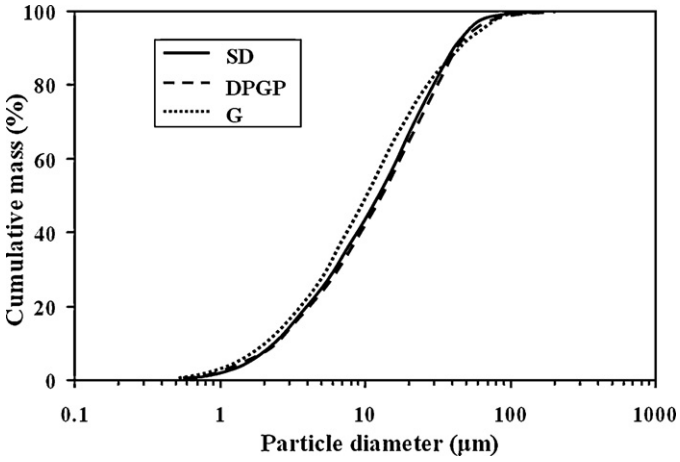

Fig. 3. Particle size distribution of the powders obtained by the three studied processes.

2.3. Characterization of the granules

2.3.1. Bulk density and flowability

Ceramic powder was filled into a measuring cylinder through a funnel, avoiding any vibration. The cylinder was then gently tapped until a constant volume was obtained. Powder weight and volume before and after tapping were measured to calculate free-fall bulk density and tapped bulk density, respectively, the ratio of the former to the latter (Hausner ratio) being calculated to evaluate powder flowability [10]. A powder charge was also placed in a timer-equipped stainless steel funnel with inner dimensions of 155 mm dia. (at top) × 10 mm dia. (at bottom) × 150 mm height, and the volume flow velocity was calculated in order to evaluate flowability in a different way [11].

2.3.2. Granule size distribution, pore size distribution, morphology, microstructure, and apparent yield pressure

Fifty gram of each powder was dried at 110 °C for 2 h and screened through grading sieves, using a mechanical vibrator under controlled conditions. Every screen residue was weighed to evaluate the granule size distribution of the powders.

The predominant granule size range (300–500 μm) was selected for the determination of granule characteristics. These were determined as follows:

- Intragranular pore size distribution was determined by mercury intrusion porosimetry.
- Granule morphology was observed with a digital optical microscope.
- Intragranular microstructure was determined on polished cross-sections of granules mounted in epoxy, using a scanning electron microscope (SEM) [1].
- Granule strength was evaluated by determining the apparent yield pressure, P_y [1,12–14]. For this, the granule samples were adjusted to a moisture content of 0.055 kg water/kg dry solid and stored for 24 h. Compaction curves were prepared by compacting 2 g samples of the granules at a rate of 2 mm/min in a cylindrical steel die, 18.9 mm in diameter, using a

universal testing machine. Load and displacement were automatically recorded up to a maximum pressure of 40 MPa. The log pressure–compactness response (compaction curve) was calculated from the load–displacement curve. Corrections for springback were made as described by Mort et al. [15]. Apparent yield pressure, P_y, was determined from the intersection of two straight lines fitted to the low-pressure and high-pressure legs of the compaction curve [1,12,13].

2.4. Pressing and characterization of the compacts

2.4.1. Pressing of the compacts

The test powders, with a moisture content of 0.055 kg water/kg dry solid, were stored for 24 h before pressing. A uniaxial press with an 80 mm × 20 mm rectangular die was used, adjusting die depth to obtain 7.0 ± 0.1 mm thick compacts. Compacts were pressed, first, at 15, 25, and 40 MPa of each type of powder and dried at 110 °C to constant weight. Compact bulk density was then determined. The dry bulk density data of the pressed compacts were then plotted versus pressing pressure to determine powder pressing behaviour.

Compacts were also prepared with a bulk density of 2.00 g/cm^3, pressed at 32.5 MPa, from the SD powder as a reference, because this is approximately the green bulk density of ceramic tiles manufactured in industrial practice. Compacts were additionally pressed from the DPGP powder, at 29.0 MPa, and from the G powder, at 15.5 MPa, to the same bulk density of 2.00 g/cm^3. A further series of compacts were also pressed from the DPGP and G powders at 32.5 MPa. This enabled a comprehensive comparison to be carried out of the compacts obtained at the same bulk density and at the same pressing pressure.

2.4.2. Bending strength, microstructure, and pore size distribution

All compacts (10 of each sample) were dried at 110 °C for 12 h, after which their bending strength was determined by three-point bending with a 61.25 mm span at a crosshead speed of 10 mm/min. The microstructure of the compact cross-sections was observed by SEM. The pore size distribution of the compacts was determined by mercury intrusion porosimetry.

3. Results and discussion

3.1. Granule characterization

3.1.1. Granule size distribution

The granule size distributions of the three granulated powders and of the non-granulated powder prepared from the same starting composition are shown in Fig. 4. The DPGP powder exhibited a similar granule size distribution to that of the SD powder, with a slight shift to larger granule sizes. In contrast, the G powder displayed a much larger coarse fraction.

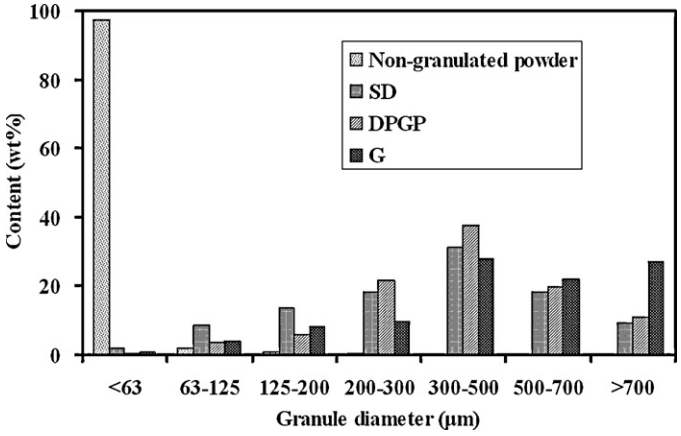

Fig. 4. Granule size distributions of the powders.

3.1.2. Flowability and morphology

Table 2 details the free-fall and tapped bulk densities of the powders, together with their Hausner ratio and volume flow velocity. The granulated SD, DPGP, and G powders displayed similar bulk density and flowability, which were much higher than those of the non-granulated powder. However, clear differences in bulk density and flowability were also to be observed among the three granulated powders.

The Hausner ratio and volume flow velocity indicate that the DPGP powder was slightly more flowable than the G powder, but less flowable than the SD powder. Since the granule sizes of the DPGP, SD, and G powders lay in a similar range (Fig. 4), the difference in flowability was mainly attributable to the difference in granule shapes. Fig. 5 shows that the SD granules had a spherical shape, while the DPGP and G granules had irregular shapes, which explain the small differences in flowability.

3.1.3. Bulk density, microstructure, and pore size distribution

Powder bulk density accounts for both the true density of the raw material particles and the total volume of the interstitial voids between the particles, which consist of intergranular pores (spaces between the granules during powder packing) and intragranular pores (inter-particle spaces in the granules). Since the same starting composition was used to prepare each powder, the true density of the raw material particles may be treated as constant. Therefore, the differences in the studied powder bulk

Table 2
Bulk density and flowability of the powders.

Powder	Free-fall bulk density (g/cm^3)	Tapped bulk density (g/cm^3)	Hausner ratio	Volume flow velocity (cm^3/s)
SD	1.11 ± 0.01	1.35 ± 0.01	1.21	16.6 ± 0.1
DPGP	1.08 ± 0.01	1.32 ± 0.01	1.23	14.9 ± 0.1
G	1.23 ± 0.02	1.53 ± 0.02	1.25	14.5 ± 0.1
Non-granulated powder	0.68 ± 0.01	1.08 ± 0.01	1.58	Non-flowing

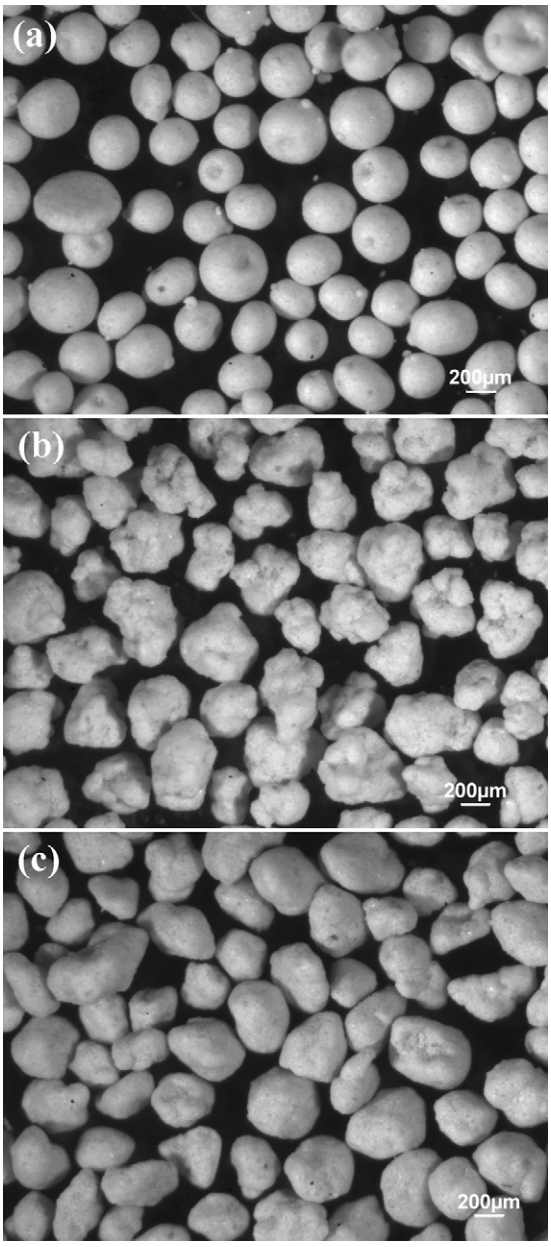

Fig. 5. Morphology of (a) SD, (b) DPGP, and (c) G granules. Granule size range: 300–500 μm.

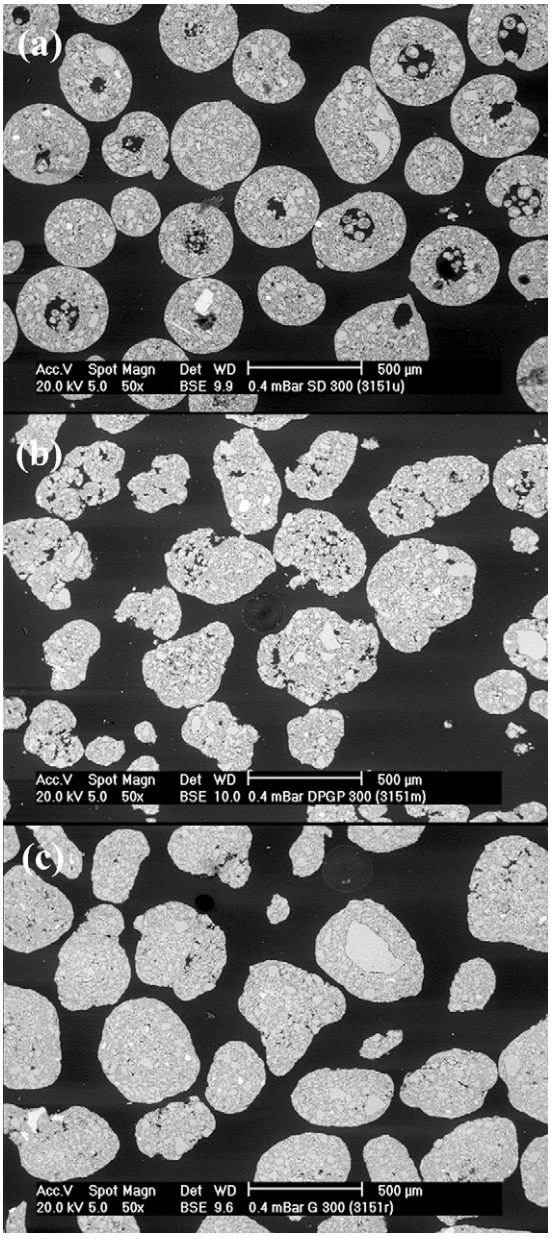

Fig. 6. Cross-sections of (a) SD, (b) DPGP, and (c) G granules. Granule size range: 300–500 μm.

densities mainly depended on the total volume of the intergranular and intragranular pores.

In a free-fall powder bed, intergranular pore volume is influenced by granule size distribution and granule sphericity. In similar granule size distributions (Fig. 4), granule sphericity was the main factor affecting intergranular pore volume: greater granule sphericity generally leads to lower intergranular pore volume and, hence, higher powder bulk density. Fig. 5 shows that the SD granules exhibited the greatest sphericity, whereas the DPGP and G granules displayed irregular shapes. It may be observed in Table 2, however, that SD powder bulk density (1.11 g/cm^3) was almost the same as that of the DPGP powder (1.08 g/cm^3), while both were much lower than that of the G powder (1.23 g/cm^3), indicating that, in addition to intergranular pore volume, intragranular pore volume also played a significant role in powder bulk density.

Fig. 6 displays polished cross-sections of the SD, DPGP, and G granules. The SD granules resembled ‘‘hollow’’ aggregations with a large internal cavity (up to 200 μm). According to the literature, this is due to migration of the inner particles to the outer shell with capillary-induced water migration in the deflocculated slurry droplet during spray drying [16–18]. The large internal cavity may be considered an intergranular pore and would thus notably increase the total intergranular pore volume of the SD powder and decrease its bulk density. The DPGP granules resembled ‘‘solid’’ aggregations, produced by the DPGP granulation process in which slurry droplets adsorbed fine dry powders to form solid granules that were

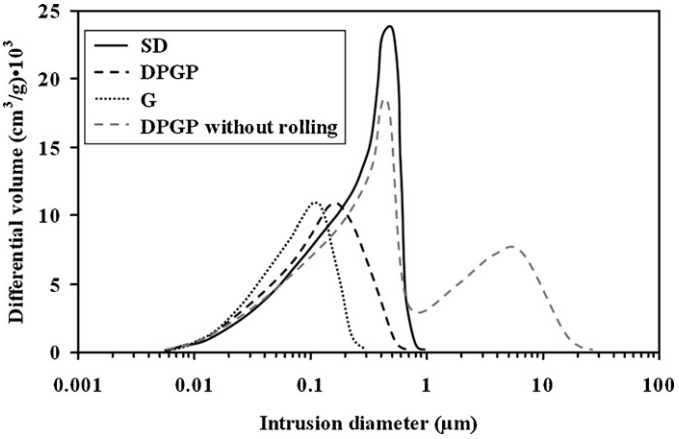

Fig. 7. Intragranular porosity distributions of SD, DPGP, and G granules. Granule size range: 300–500 μm.

then subjected to rolling treatment to produce the final granules. The randomly distributed, distinguishable voids (up to 60 μm) inside the DPGP granule were deemed to be the remaining interspaces between the finer raw granules that assembled into the final coarser granules during rolling (discussed in detail in Section 3.1.5). The G granules resembled denser ''solid'' aggregations, produced by the G process, in which fine dry powders agglomerated during wet agitation to form solid granules. In comparison with the DPGP granules, the G granules displayed inner voids that were much less distinguishable and were also deemed to be the interspaces remaining between the initial finer granules that assembled into the final coarser granules during G granulation.

The intragranular pore size distributions of the SD, DPGP, and G granules are plotted in Fig. 7 and the total intragranular pore volumes are detailed in Table 3. Pores larger than 20 μm were found, but these are not displayed in Fig. 7 or counted in Table 3 because they were assumed to correspond to the spaces between the granules in the powder bed or to the inner voids of the SD granules.

It may be observed that the most frequent pore size (Fig. 7) and the total intragranular pore volume (Table 3) both decreased in the order: SD, DPGP, and G, indicating that granule compactness increased in this order.

The high compactness of the G granules may be attributed, in the first place, to the high packing density of the clay particles in the dry starting G powder composition. Since the raw materials were dry ground by pendulum milling and handled as dry powders (without dispersion in water), many clay particles existed as dense agglomerates, which stemmed from the raw clay mineral. At the same time, the presence of agglomerates provided a wide clay particle size distribution, yielding high particle packing density. G granule high compactness was, secondly, due to the highly intensive agitation and mechanical compaction of the granules in the mixer-granulator.

DPGP granule compactness may be mainly attributed to the DPGP mechanical compaction of the granules during rolling treatment, in view of the significant change in intergranular pore volume between the rolled DPGP granules (0.13 cm^3/g) and the non-rolled DPGP granules (0.22 cm^3/g), detailed in Table 3.

In the SD granules, particle movement, owing to water migration, and the ensuing particle enrichment at the outer shell contributed to SD granule compactness.

In short, it may be concluded that the G powder had the highest free-fall bulk density (1.23 g/cm^3) since the granules displayed the greatest compactness, while the SD and DPGP powders had lower free-fall bulk density (1.11 and 1.08 g/cm^3 respectively) owing to lower granule compactness and the highly irregular shape of the DPGP granules.

3.1.4. Apparent yield pressure

Table 3 also shows the apparent yield pressure, i.e. mechanical strength, of the SD, DPGP, and G granules. The three types of granules displayed similar mechanical strength, though certain differences were to be observed. The G granules exhibited the highest apparent yield pressure (0.32 MPa), as they had the highest compactness (lowest intragranular pore volume, 0.09 cm^3/g) and most solid structure (Fig. 6).

However, though the SD granules displayed higher porosity (0.17 cm^3/g) and a hollower structure (Fig. 6) than the DPGP granules (porosity 0.13 cm^3/g), they exhibited higher mechanical strength (0.28 and 0.22 MPa, for SD and DPGP respectively). This may be attributed to the rigid shell of the SD granules. Studies [13–15] have shown that, during the spray-drying process, owing to the intensive capillary-induced water flow, inner clay particles and deflocculants are drawn to the droplet surface to form a rigid shell, benefiting from the ensuing clay particle compaction and clay and deflocculant binding behaviour. The final SD granules thus exhibited higher

Table 3
Granule characteristics in the studied granule size range (300–500 μm) and resulting compact characteristics.

Powder	Granules		Compacts			
	Intragranular pore volume (cm^3/g)	Apparent yield pressure, P_y (MPa)	Pressed to the same dry bulk density of 2.00 g/cm^3		Pressed at the same pressure of 32.5 MPa	
			Dry bulk density (g/cm^3)	Bending strength (MPa)	Dry bulk density (g/cm^3)	Bending strength (MPa)
SD	0.17 ± 0.02	0.28 ± 0.03	2.001 ± 0.002	3.4 ± 0.1	2.001 ± 0.002	3.4 ± 0.1
DPGP	0.13 ± 0.01	0.22 ± 0.02	2.002 ± 0.002	3.0 ± 0.1	2.020 ± 0.002	3.2 ± 0.1
G	0.09 ± 0.01	0.32 ± 0.03	2.002 ± 0.002	1.8 ± 0.1	2.094 ± 0.001	2.8 ± 0.1
DPGP without rolling	0.22 ± 0.02	0.09 ± 0.01	–	–	–	–

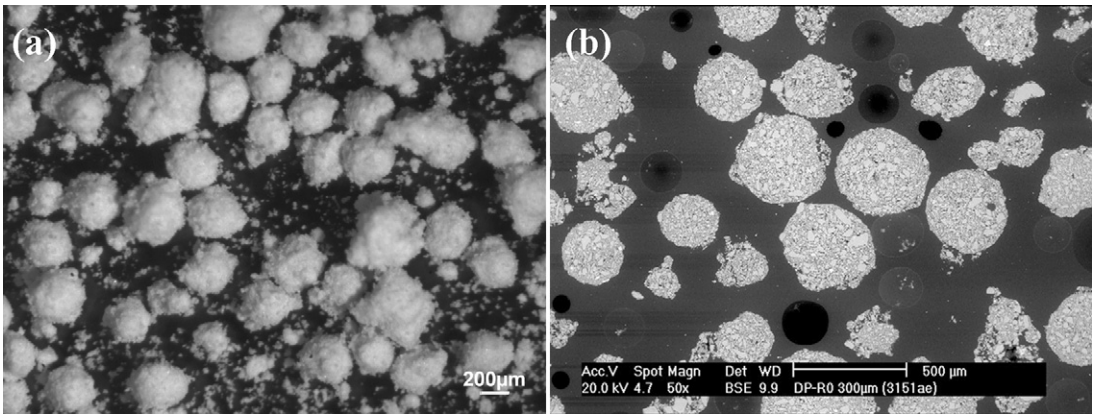

Fig. 8. (a) Morphology and (b) cross-sections of DPGP granules without rolling treatment.

mechanical strength than the DPGP granules, in which the water flow was much less intensive, leading to much weaker binder (clay and deflocculant) enrichment at the granule surface. In addition, the acetic acid used as a flocculant in the DPGP filter-pressing step remained partly in the DPGP granules. Owing to the very small molecule size of acetic acid, however, it was not deemed to act as a binder or to contribute to DPGP granule strength.

3.1.5. Evolution of granule morphology in the DPGP process

In this section, the non-rolled raw DPGP granules obtained from spray-mixing were characterized, in contrast to the rolled DPGP granules studied above.

The morphology and cross-sections of non-rolled DPGP granules are presented in Fig. 8. It shows that during the spray-mixing stage the fine dry powders were loosely adsorbed onto the slurry droplet to form granules with a spherical shape and flocky surface. The intragranular pore size distribution of the non-rolled DPGP powder is plotted in Fig. 7. This shows that there were a significant number of large pores sized 1–10 μm, corresponding to the voids between the fine powders at the flocky surface layer of the non-rolled DPGP granules (Fig. 8a).

The results indicate that rolling acted as an effective compacting process, smoothing the DPGP granule surface (Fig. 5b), reducing intragranular pore size (Fig. 7) and pore volume (from 0.22 to 0.13 cm^3/g), and raising granule mechanical strength (apparent yield pressure, from 0.09 to 0.22 MPa).

Granule size distribution before and after rolling is depicted in Fig. 9. It shows that DPGP granule size distribution shifted to much larger granule sizes after rolling. In addition to compacting, rolling therefore also served as a granulating process, agglomerating finer granules into coarser granules, thus producing the combined-ball shape of the final rolled DPGP granules (Fig. 5b) and the distinguishable voids inside the rolled DPGP granules (Fig. 6b).

In short, the rolling treatment played a major role in the formation of the DPGP granules and provided particle compaction in addition to surface smoothing, higher mechanical strength, a larger size, and more irregular shapes of the DPGP granules.

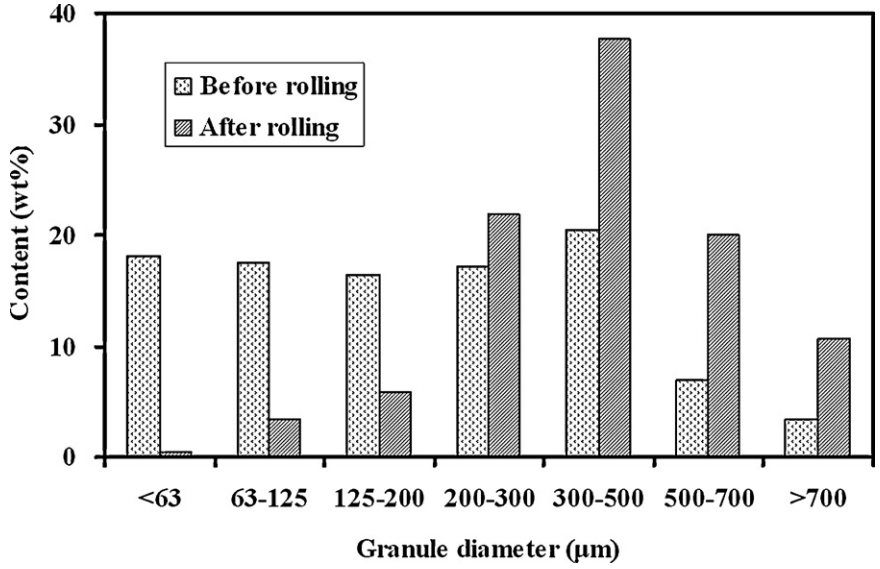

Fig. 9. Granule size distribution of DPGP powders before and after rolling.

3.2. Characterization of the compacts

3.2.1. Pressing behaviour

The pressing behaviour of the SD, DPGP, and G powders is shown in Fig. 10. The dry bulk densities of the compacts are detailed in Table 3. It shows that, to obtain compacts with the same bulk density, pressure needed to be raised in the order: G, DPGP, and SD. Similarly, when pressed at the same pressure, compact dry bulk density decreased in the order: G, DPGP, and SD. The DPGP granule behaviour resembled the SD granule behaviour more closely than the G granule behaviour. The differences in granule compactness (intragranular pore volume) and apparent yield pressure of the three studied powders (Table 3) indicate that compact bulk density depended more on granule compactness than on apparent yield pressure.

3.2.2. Compacts pressed to the same bulk density (2.00 g/cm^3)

The porosity distributions of the compacts pressed to the same bulk density (2.00 g/cm^3) from the different studied powders at different pressures (SD at 32.5 MPa, DPGP at 29.0 MPa, and G at 15.5 MPa) are plotted in Fig. 11a. The porosities of the three compacts were similar in the small-pore fraction (0.01–0.1 μm) but quite different in the large-pore fraction (1–10 μm): that is, the quantity and size of the large pores increased in the order: SD, DPGP, and G.

The same trend was found in the SEM observation of the compact microstructures; a typical example of each is shown in Fig. 12. The SD compacts (Fig. 12a) exhibited the most homogeneous particle arrangement, while the G compacts (Fig. 12c) retained distinguishable granule boundaries at which large pores appeared. The DPGP compact (Fig. 12b) exhibited an intermediate appearance with some distinguishable granule boundaries.

Since there was a remarkable increase in pressing pressure in the order: G (15.5 MPa), DPGP (29.0 MPa), and SD (32.5 MPa), as shown in Fig. 10, the differences in porosity distribution and microstructure may be attributed to the differences in pressing pressure: the higher the pressing pressure, the greater the granule deformation and, hence, the blurrier the residual granule boundary and the smaller the large-pore size in the compact.

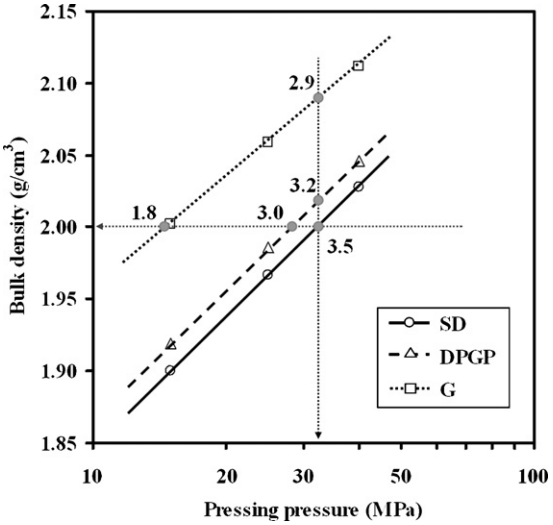

Fig. 10. Bulk density versus pressing pressure of the dry compacts. The numbers inside the graph correspond to the bending strength of the compacts at each cross point, expressed in MPa.

3.2.3. Compacts pressed at the same pressure (32.5 MPa)

When pressed at the same pressure (32.5 MPa), the DPGP and G compacts still exhibited larger pores than the SD compacts (Fig. 11b), while the G compacts also displayed much clearer residual granule boundaries than the SD and DPGP compacts (Fig. 12a, d, and e). In addition to pressing pressure, granule characteristics therefore also played an important role in the resulting compact microstructure.

During pressing, the intragranular and particularly the intergranular pores in the packed powder were progressively

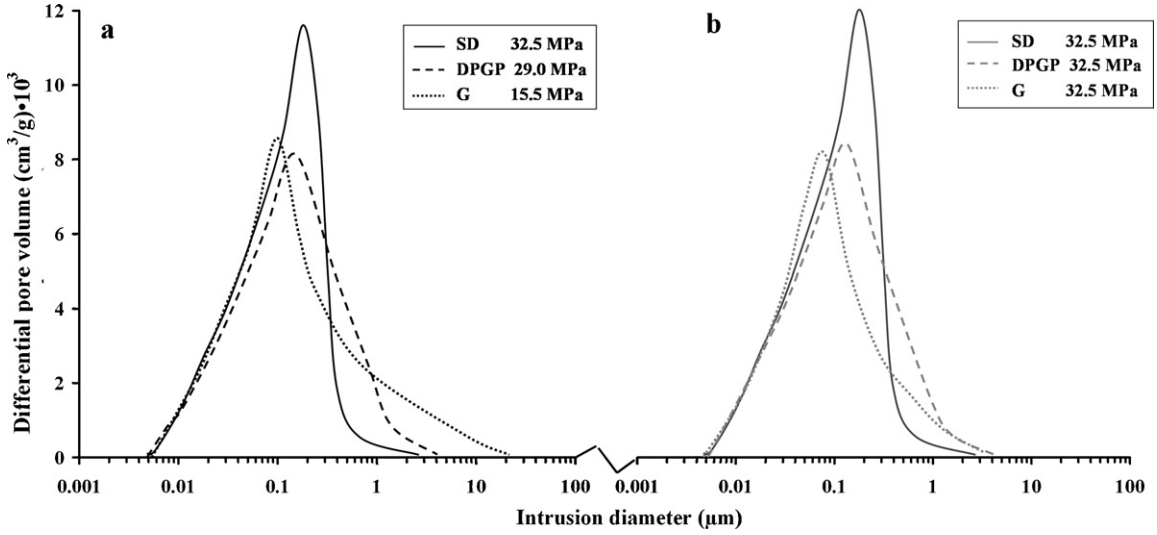

Fig. 11. Porosity distribution of the SD, DPGP, and G compacts: (a) pressed to the same bulk density (SD granules at 32.5 MPa, DPGP granules at 29.0 MPa, and G granules at 15.5 MPa) and (b) pressed at the same pressure of 32.5 MPa.

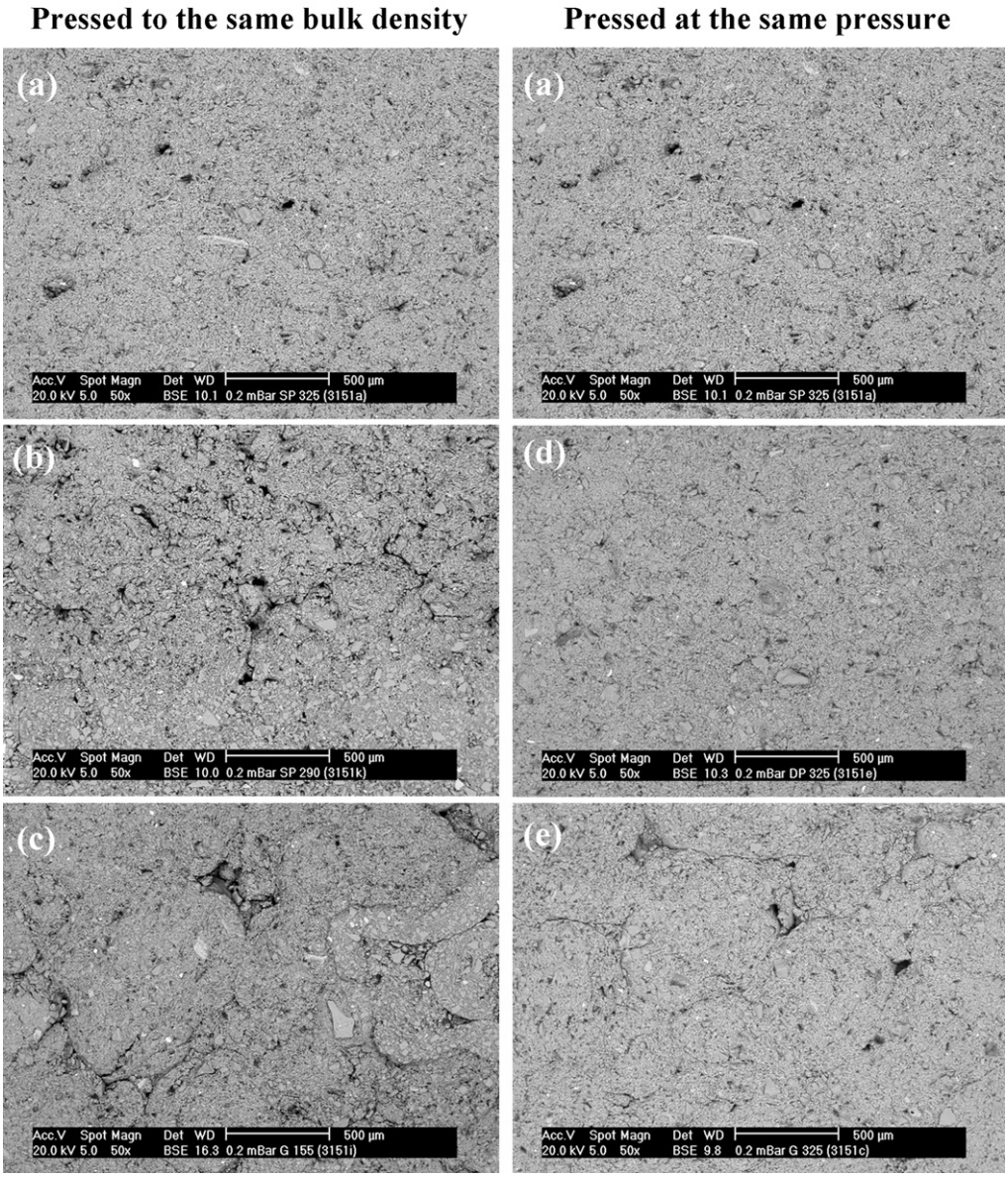

Fig. 12. Microstructure of the SD, DPGP, and G compacts: pressed to the same bulk density (a) SD granules at 32.5 MPa, (b) DPGP granules at 29.0 MPa, and (c) G granules at 15.5 MPa; and pressed at the same pressure (a) SD granules at 32.5 MPa, (d) DPGP granules at 32.5 MPa and (e) G granules at 32.5 MPa.

eliminated by granule deformation. Furthermore, since the intragranular pores were smaller than 1 μm (Fig. 7), they were the intergranular pores that gave rise to the large pores (>1 μm) in the compacts (Fig. 11). Therefore, granule deformability, which influences pore elimination during pressing, has a crucial effect on the residual intergranular porosity and microstructure of the pressed compacts, and, higher granule deformability may be expected to lead to lower proportion of residual large pores (>1 μm) and blurrier residual granule boundaries in the compacts.

Figs. 11b and 12 show respectively that, much lower proportion of large pores (>1 μm) were retained in the SD compacts than in the DPGP and G compacts, and, much clearer granule boundaries were retained in the G compacts (Fig. 12e) than in the SD and DPGP compacts (Fig. 12a and d), indicating that granule deformability decreased in the order: SD, DPGP and G. In view of the differences in porosity and apparent yield pressure of the three studied powders (Table 3), granule deformability was deemed to depend more on granule compactness than on granule apparent yield pressure.

3.2.4. Bending strength

Fig. 10 and Table 3 also present the bending strength of the SD, DPGP, and G compacts pressed either to the same bulk density (2.00 g/cm^3) or at the same pressure (32.5 MPa).

For the studied powder compacts, formed under either pressing condition, bending strength always increased in the order: G, DPGP and SD as a result of the decrease in pore size and residual granule boundaries in the order: G, DPGP, and SD (Figs. 11 and 12), because the large pores and cracks

(corresponding to residual granule boundaries) were microstructural defects that reduced the bending strength of the materials [12,19–21].

4. Conclusions

In this study, a recently proposed new ceramic powder preparation process, the droplet–powder granulation process (DPGP), was analysed and the granules and resulting pressed green compacts were characterized and compared with those obtained using traditional spray-drying (SD) and granulation (G) processes.

The spray-mixing step yielded spherical granules with a flocky surface. The subsequent rolling treatment played a major role in DPGP granule evolution by compacting the particles, smoothing the surface, increasing granule apparent yield pressure and size, and making the shape less regular. The final DPGP powder consisted of irregularly shaped solid granules with a combined-ball shape, and had a similar granule size distribution and bulk density to those of the SD powder. Powder flowability and granule compactness of the DPGP powder were intermediate between those of the SD and G powders, while granule apparent yield pressure increased, with minor differences, in the order: DPGP, SD, and G.

When the granules were pressed at the same pressure, the dry bulk density of the DPGP compacts was intermediate between that of the SD and G compacts, indicating that compact dry bulk density depended more on granule compactness than on granule apparent yield pressure. Granule deformability decreased in the order: SD, DPGP, and G, with a corresponding increase in large intergranular pore sizes and residual granule boundaries in the resulting pressed compacts. These microstructural defects reduced the compact bending strength.

The study shows that the DPGP process, in which more stages are used in order to make it cleaner than the SD process, yields granules and green compacts with suitable properties for porcelain tile manufacture. A further research study will examine the firing behaviour and final properties of porcelain tiles obtained with this new technology.

Acknowledgements

This study benefits from the international cooperation between China University of Geosciences (CUG, China) and the Instituto de Tecnología Cerámica (ITC) at Universitat Jaume I (UJI, Spain). The Chinese Scholarship Council is also gratefully thanked for its financial support (File No. 2009641029).

References

[1] J.L. Amoros, V. Cantavella, J.C. Jarque, C. Feliu, Fracture properties of spray-dried powder compacts: effect of granule size, J. Eur. Ceram. Soc. 28 (2008) 2823–2834.
[2] J.L. Amoros, M.J. Orts, J. Garcia-Ten, A. Gozalbo, E. Sanchez, Effect of the green porous texture on porcelain tile properties, J. Eur. Ceram. Soc. 27 (2007) 2295–2301.
[3] M. Radeka, J. Ranogajec, R. Marinkovic-Neducin, B. Zivanovic, Compaction mechanism as the function of atomized powder particle size, Ceram. Int. 21 (1995) 249–255.
[4] H.J. Alves, F.G. Melchiades, A.O. Boschi, Effect of spray-dried powder granulometry on the porous microstructure of polished porcelain tile, J. Eur. Ceram. Soc. 30 (2010) 1259–1265.
[5] E. Sánchez, J. García-Ten, V. Sanz, A. Moreno, Porcelain tile: almost 30 years of steady scientific-technological evolution, Ceram. Int. 36 (2010) 831–845.
[6] IPTS. Reference document on best available techniques in the ceramic manufacturing industry, European Commission (http://eippcb.jrc.es/reference/cer.html) (2007) 116.
[7] M.C. Minguillón, E. Monfort, X. Querol, A. Alastuey, I. Celades, J.V. Miró, Effect of ceramic industrial particulate emission control on key components of ambient PM(10), J. Environ. Manage. 90 (8) (2009) 2558–2567.
[8] M.C. Minguillón, X. Querol, A. Alastuey, E. Monfort, E. Mantilla, M.J. Sanz, F. Sanz, A. Roig, A. Renau, C. Felis, J.V. Miró, B. Artiñano, PM10 speciation and determination of air quality target levels. A case study in a highly industrialized area of Spain, Sci. Total Environ. 372 (2007) 382–396.
[9] Z. Shu, J. Zhou, Y.X. Wang, A novel approach of preparing press-powders for cleaner production of ceramic tiles, J. Clean. Prod. 18 (2010) 1045–1051.
[10] E.C. Abdullah, D. Geldart, The use of bulk density measurements as flowability indicators, Powder Technol. 102 (1999) 151–165.
[11] A. Santomaso, P. Lazzaro, P. Canu, Powder flowability and density ratios: the impact of granules packing, Chem. Eng. Sci. 58 (2003) 2857–2874.
[12] S. Balasubramanian, D.J. Shanefield, D.E. Niesz, Effect of internal lubricants on defects in compacts made from spray-dried powders, J. Am. Ceram. Soc. 85 (2002) 134–138.
[13] S. Balasubramanian, D.J. Shanefield, D.E. Niesz, Effect of externally applied plasticizer on compaction behavior of spray-dried powders, J. Am. Ceram. Soc. 85 (2002) 749–754.
[14] J.H. Song, J.R. Evans, A die pressing test for the estimation of agglomerate strength, J. Am. Ceram. Soc. 77 (1994) 806–814.
[15] P.H. Mort, R. Sabia, D.E. Niesz, R.E. Riman, Automated generation and analysis of powder compaction diagrams, Powder Technol. 79 (1994) 111–119.
[16] W.J. Walker Jr., J.S. Reed, Influence of slurry parameters on the characteristics of spray-dried granules, J. Am. Ceram. Soc. 82 (1999) 1711–1719.
[17] S.J. Lukasiewicz, Spray-drying ceramic powders, J. Am. Ceram. Soc. 72 (1989) 617–624.
[18] G. Bertranda, P. Roya, C. Filiatreb, C. Coddeta, Spray-dried ceramic powders: a quantitative correlation between slurry characteristics and shapes of the granules, Chem. Eng. Sci. 60 (2005) 95–102.
[19] D. Bortzmeyer, G. Langguth, D. Orange, Fracture mechanics of green products, J. Eur. Ceram. Soc. 11 (1993) 9–16.
[20] Z. Zhang, D.J. Green, Fracture toughness of spray-dried powder compacts, J. Am. Ceram. Soc. 85 (2002) 1330–1332.
[21] M. Uppalapati, D.J. Green, Effect of relative humidity on the viscoelastic and mechanical properties of spray-dried powder compacts, J. Am. Ceram. Soc. 89 (2006) 1212–1217.